Testing the Validity of Lamberts Law for Micro-scale Photometric Stereo Applied to Paper Substrates

Faisal Azhar[1], Khemraj Emrith[2], Stephen Pollard[1], Melvyn Smith[2], Guy Adams[1] and Steve Simske[3]
[1]*Hewlett Packard Laboratories, Bristol, U.K.*
[2]*Centre for Machine Vision, University of West of England, Bristol, U.K.*
[3]*Hewlett Packard Laboratories, Ft Collins, U.S.A.*

Keywords: Micro-scale Photometric Stereo, Lambert Reflectance Model, Paper and Surface Normals.

Abstract: This paper presents an empirical study to investigate the use of photometric stereo (PS) for micro-scale 3D measurement of paper samples. PS estimates per-pixel surface orientation from images of a surface captured from the same viewpoint but under different illumination directions. Specifically, we investigate the surface properties of paper to test whether they are sufficiently well approximated by a Lambertian reflectance model to allow veridical surface reconstruction under PS and explore the range of conditions for which this model is valid. We present an empirical setup that is used to conduct a series of experiments in order to analyse the applicability of PS at the micro-scale. In addition, we determine the best 4, 6, and 8 light source tilt (illumination) angles with respect to multi-source micro-scale PS. Furthermore, an intensity based image registration method is used to test the accuracy of the recovery of surface normals. The results demonstrate that at the micro-scale: (a) Lambert model represents well the data sets with low root mean square (RMS) error between the original and reconstructed image, (b) increasing the light sources from 4 to 8 reduces RMS error, and (c) PS can be used to extract veridical surface normals.

1 INTRODUCTION

Photometric stereo (PS) has been widely used at macro-scale to recover local surface orientation and reflectance properties of a surface by using various reflectance models such as Lambertian, Phong, Torrance-Sparrow, Cook-Torrance, Oren-Nayar etc. (Matsushita and Ikeuchi, 2012; McGunnigle et al., 2012; Yang and Ahuja, 2012). The local surface orientation obtained at each pixel can be integrated to create a detailed 3D surface reconstruction (Li and Li, 2011). The PS method is simple and uses per pixel surface reconstruction with time efficacy and has the advantage, over conventional stereo vision, that it does not require solving a correspondence problem (Angelopoulou and Petrou, 2013; Gorpas et al., 2013; Li and Li, 2011). The applications include surface inspection, fault detection, shape recovery, recognition, biometrics, quality assurance, auditing, charge allowance etc. (Bringier et al., 2012; Li and Li, 2011). There have been limited applications of photometric stereo at the micro scale (Gorpas et al., 2013; Johnson et al., 2011; Li and Li, 2011). This is because at micro-scale the general assumptions of the standard PS are violated, i.e., light sources are close to the surface, light is not uniformly distributed and the surface reflectance may not be approximated by Lambert's law.

We investigate whether the surface of paper is sufficiently well described as Lambertian at the micro-scale. We are surrounded by paper from routine and private documents to bank notes, flyers, posters, tickets, etc. The frequent and numerous routine usage of paper makes its surface topography inspection vital for the paper and printing industry. The surface topography of paper can be used to assess paper and print characteristics such as ink transfer, ink distribution, and surface gloss, it can also be used to authenticate the paper itself etc. (Chinga-carrasco, 2012; Clarkson et al., 2009; Kuparinen et al., 2007; Pino and Pladellorens, 2009). In this context, we apply multi-source PS based on Lambertian model to three paper types, i.e., embossed, gloss and matte, to verify whether Lambert's model fits well at the micro-scale. Data sets are obtained by using an optical microscope with a 5MP digital camera to image paper samples on a platform suspended above a rotating white light

Azhar F., Emrith K., Pollard S., Smith M., Adams G. and Simske S..
Testing the Validity of Lamberts Law for Micro-scale Photometric Stereo Applied to Paper Substrates.
DOI: 10.5220/0005359302460253
In *Proceedings of the 10th International Conference on Computer Vision Theory and Applications* (VISAPP-2015), pages 246-253
ISBN: 978-989-758-089-5

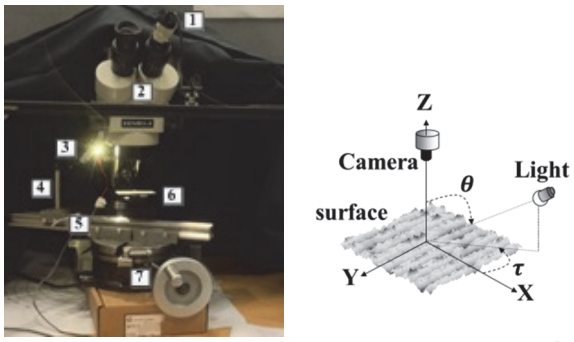

Figure 1: Experimental setup on left with numbered (1) 5MP digital camera, (2) an optical microscope, (3) LED light source, (4) and (5) vertical and horizontal adjustment of LED from paper sample placed on a platform (6), and (7) turntable to rotate the LED. The corresponding setup on the right represent photometric stereo image capture.

source as shown in Figure 1. The datasets provide photometric images captured at different light source tilt angles (labelled τ in Figure 1) for each paper type together with variations in the horizontal and vertical distances of the light sources from the paper sample (which affect its slant angle θ). Through this setup we investigate whether paper is well approximated by a Lambertian reflectance model at the micro-scale. Next, we investigate the use of 4, 6 and 8 light source PS for micro-scale recovery of local surface orientation. To the authors knowledge this is the first work to determine optimal illumination positions from more than three PS (Drbohlav and Chantler, 2005 does it for 3 PS), i.e., 4, 6 and 8 light sources, by comparing each choice with "reference data" that is obtained by applying PS to the complete set of 49 and 55 photometric images. Finally, we investigate whether PS can provide robust veridical surface normals from micro-scale paper images. We utilize an intensity based image registration to align PS images for a paper rotated in the x-y plane through roughly 45 degrees and directly compare the recovered surface gradients/normals.

The major contributions of this study are as follows: (a) implementation of a Sine curve model fit for local (per-pixel) and global (image) data to establish whether paper is Lambertian at the micro-scale, (b) design of a procedure to determine best tilt angles for 4, 6, and 8 light source micro-scale PS, and (c) utilisation of an intensity based image registration method to verify the geometrical accuracy of the recovered surface normals. This paper is organized as follows. Section II reviews the literature. Section III briefly describes the PS method. Section IV presents experimental investigation, results and discussions. Section V concludes the paper.

2 LITERATURE REVIEW

2.1 Macro-scale PS

Macro-scale PS methods can be divided into two categories based on the understanding whether the non-Lambertian reflections are considered as outliers for removal, or as inliers within a non-linear reflectance model (Ikehata et al., 2014; McGunnigle et al., 2012; Yang and Ahuja, 2012).

The first category assumes a Lambertian reflectance model and incorporates an outlier detection algorithm for handling non-Lambertian pixels or regions in an image (Woodham, 1980), (Barsky et al., 2003; Coleman and Jain, 1982; Sun et al., 2007). Traditional PS methods based on Lambert's law require at least three images of a surface taken from the same viewpoint but with different illumination. Coleman and Jain, 1982, extend Woodham, 1980, original approach by employing a fourth light source. They recover surface normals using the image triplets that produce the lowest albedos assuming that triplets with higher albedos must be affected by the specular reflection and that the specular reflections in different images do not intersect. This method fails to recover the surface normals accurately in the presence of shadows and highlights. Barsky et al., 2003, addressed this limitation by using colour projection and detecting both specular reflections and shadows. Sun et al., 2007, simplified the method of Barsky et al., 2003, by detecting and eliminating specular (highest intensity value) and shadow (lowest intensity value) pixels from six photometric images to recover surface normals. These methods are computationally expensive due to the per-pixel computations required to choose from the increasingly large sets of photometric images used (Wu and Tang, 2010; Yang and Ahuja, 2012).

The second category considers non-Lambertian reflections as inliers and defines reflectance models e.g., Phong, Torrance-Sparrow, Cook-Torrance etc. Phong reflectance model is a linear combination of diffuse (Lambertian), specular, and ambient components (Argyriou, Vasileios and Petrou, 2008). The Torrance-Sparrow and Cook-Torrance models consider surface micro-facets as a combination of ''V-shaped" cavities (Cook and Torrance, 1982; Torrance and Sparrow, 1967). While they are designed for specular surfaces they are also able to represent rough materials whose surface properties

are different from the Lambertian model. However, these methods suffer from the effects of shadows and numerical instabilities derived from the complex non-linear optimization required for their solution (Ikehata et al., 2014). McGunnigle et al. (2012), use Oren-Nayar reflectance model, which also considers a surface as a combination of micro-facets, to model the behaviour of matte surfaces that violate Lambert's Law. The authors compute intensity contributed from all the individual facets of the surface and present a qualitative model which works well provided the surface roughness is <0.3. More recently the use of general reflectance properties such as monotonicity, visibility, and isotropy, that are common among reflections from diverse materials, has been suggested in order to apply PS to a wide range of materials (Higo et al., 2010). However, even this method is not able to deal with the reflectance function whose specular component is composed of two or more lobes.

2.2 Micro-scale PS

Johnson et al., 2011, developed an elastomeric sensor and applied PS that uses six LEDs to capture microscopic structure of surface materials independent of their surface properties. However, besides being expensive, bulky and slow, the sensor is also not appropriate for non-rigid surfaces and does not recover the albedo or other surface properties of the material. Li and Li, 2011, claim to be the first to apply uncalibrated PS for microstructure 3D measurement. They use generalized bas-relief to resolve the inherent shape or light ambiguity of uncalibrated PS. They use a Markov Random Field based graph cuts energy minimization model to refine the recovered surface normals. Their method has been shown to work well on synthetic data and real images (640 x 480 pixels and 1024 x 768 pixels). However, the computational complexity of this method is not presented. Hence, it is not known if this method is suitable for real-time and real-world application. Recently, a miniature PS system (Gorpas et al., 2013) has been proposed for textile surface reconstruction. It uses a low-cost camera (640 x 480 pixels) with eight LED light sources and describes hardware specifications, e.g., a cylindrical enclosure to address the ambient light and a Fresnel lens to collimate the LED illumination, in order to apply PS at the micro-scale. Furthermore, in order to ensure uniform illumination it proposes a flat-fielding procedure that normalizes the input images with images of a Lambertian surface (e.g., white paper card), with known albedo and under the same LED illumination direction. This system has been shown to recover the surfaces of textile fabrics and bank notes. However, they do not investigate whether the textile fabrics or bank notes are well approximated by the Lambertian model at the micro-scale. In fact only qualitative results were presented and neither the method nor the advantage of using 8 LED PS to reduce surface reconstruction error were explored quantitatively.

3 PHOTOMETRIC STEREO

According to Lambert's law a perfectly diffuse surface illuminated by a single distant light source appears equally bright from all viewing direction (Bringier et al., 2012). In this case, the reflected light intensity I from the surface is considered as the dot product of surface normal N and the light source illumination directions L (Argyriou, Vasileios and Petrou, 2008; Barsky et al., 2003).

$$I = \rho N \cdot L \tag{1}$$

Let us consider that $I = (\vec{I}^1\ \vec{I}^2\ \vec{I}^3 \ldots \vec{I}^k)$ and $L = (\vec{L}^1\ \vec{L}^2\ \vec{L}^3 \ldots \vec{L}^k)$ are the stack of pixel intensity and illumination vectors respectively. Here, k represents the number of illumination directions, ρ is the albedo (surface reflectance) and $N = (\vec{N}_x, \vec{N}_y, \vec{N}_z)$ are the x, y, z components of the normal at each pixel. The illumination directions L is found by computing the illumination vectors as

$$\vec{L}^k = (\sin\theta^k \cos\tau^k, \sin\theta^k \sin\tau^k, \cos\theta^k). \tag{2}$$

Where θ is the slant angle between the illumination vector and the z-axis, and τ is the tilt angle between the x-axis and the projection of the illumination vector onto the x-y plane as shown in Figure 1 right. The pseudo-inverse of the illumination direction, i.e., $[L^{-1}]$, is multiplied with the reflected intensity I in order to calculate M as

$$\rho N = [L^{-1}]I = M. \tag{3}$$

Where $M = (\vec{m}_1, \vec{m}_2, \vec{m}_3)$ is used to recover the albedo ρ by calculating the length of M as

$$\rho = \sqrt{\vec{m}_1 \circ \vec{m}_1 + \vec{m}_2 \circ \vec{m}_2 + \vec{m}_3 \circ \vec{m}_3}. \tag{4}$$

Here, "$\circ$" is element-wise product. This allows us to compute the surface normals as $N = M/\rho$. The surface gradients, i.e., p (x-direction) and q (y-direction) are determined using $p = -\vec{m}_1/\vec{m}_3$ and $q = -\vec{m}_2/\vec{m}_3$ respectively. Finally, the Frankot and Chellappa, 1988 algorithm can be used to integrate the surface gradients for 3D surface reconstruction.

4 METHODOLOGY

4.1 Experimental Setup

An optical microscope with a 5MP digital camera fitted in its eye piece is used to image paper on a platform suspended above a turntable that rotates the white LED light source at different tilt angles as shown in Figure 1. The horizontal (H) and vertical (V) distances of the light source from the centre of the paper sample (which affect its slant angle) and the light source intensity are adjustable. This setup is surrounded by a blackout cloth to avoid ambient light during the acquisition of images. Three different paper types, i.e., embossed, glossy and matte, are captured at (1280 x 960) resolution of size 4mm (width) and 3mm (height) in the experiments.

Two multi-source PS datasets of 55 and 49 images respectively, and one four source PS data set of the three paper types with different variations of light source configuration are collected. The first data set has two variations per paper type, i.e., (0.2A, H=5cm, V=6cm) and (0.3A, H=8cm, V=6cm). It contains images captured at 55 different tilt angles (from 135° to 405°) for each paper type. The second data set has three variations per paper type, i.e., (0.1A, H=2cm, V=6cm), (0.05A, H=2cm, V=4cm) and (0.05A, H=2cm, V=2cm) with images captured at 49 different tilt angles (from 140° to 380°). The specific range of tilt angles are used due to physical limitation of the experimental setup. The intensity of the light source is regulated using a current range of 0.05A to 0.40 A. The third data set has two rotation (Rot) variations of the paper sample, i.e., (0.01A, H=7cm, V=7cm, Rot=0°) and (0.01A, H=7cm, V=7cm, Rot=45°), for each paper type. It consists of photometric images taken at 4 different tilt angles (135°, 225°, 315°, and 405°).

4.2 Surface Reflectance

We present a modified Sine curve function (sinusoidal behaviour) (Saito et al., 1999) to characterise the intensity profile of paper illuminated from different tilt angles. Two multi-source data sets are used to determine whether local (individual pixels) and global (entire image) data of paper at the micro-scale is well approximated by a Lambertian reflectance model.

If the pixel intensity value at each tilt angle, τ^k, satisfies the Lambert model Equation (1) then the value must fit the Sine curve Equation (5) (Saito et al., 1999). The Sine curve fitting procedure is implemented locally and globally as follows. First, we measure how the pixel intensity values of paper surface vary with respect to different tilt angles, τ^k. Next, the surface normals N, and the surface reflectance ρ, of each pixel are estimated using PS based on Lambert's law. The Sine curve is determined by computing the intensity of each pixel, i.e., $I(\tau^k)$, at different tilt angles as

$$I(\tau^k) = \alpha \sin(\tau^k + \beta) + \gamma. \quad (5)$$

The amplitude α is derived as follows.

$$\alpha = \rho \sin\theta^k \sqrt{{N_x}^2 + {N_y}^2}. \quad (6)$$

β is the orientation of the surface normal in x-y direction, and it represents the phase shift in the sinusoidal behaviour. A modification from (Saito et al., 1999) that includes sin^{-1} is used to calculate β as

$$\beta = \sin^{-1}\left(N_x / \sqrt{{N_x}^2 + {N_y}^2}\right). \quad (7)$$

γ is computed using

$$\gamma = \rho \cos\theta^k N_z \quad (8)$$

Assuming that the paper surface is Lambertian at the micro-scale then we expect the Sine curve to fit well the reference data, i.e., recorded pixel intensity values, at the corresponding tilt angles. In addition, we can compare the reference (Original) image and the reconstructed global (entire image) data for all pixels obtained using (5) at different tilt angles, τ^k, to determine how well Lambert's model represents the paper surface at the micro-scale.

4.3 Light Source

We present a procedure to empirically determine the best 4, 6, and 8 tilt angles with respect to the reference multi-source, micro-scale PS. We use PS method in Equation (1-3) on the two multi-source PS data sets to create the reference gradients p and q in the x and y direction respectively. Let the vector $v = (1,2,\ldots k)$. A combinatorial logic is used to determine a matrix C that contains all possible non-repetitive combinations of the elements of vector v taken n at a time. Here, n is the number of selected light sources, i.e., 4, 6 and 8. Next, we select from C those combinations in which the light sources are sufficiently far apart (but not necessarily equally spaced) from each other by using

$$\tau_{low} < (\tau^{m+1} - \tau^m) < \tau_{up} \quad (9)$$

$\forall\, m = 1,2 \ldots n-1$. The lower τ_{low} and upper τ_{up} limits of difference in tilt angles between two PS

images are set as 60° and 90°, 30° and 90°, and 20° and 90° respectively to select limited combinations for $n = 4, 6$ and 8. PS is applied to each subset to compute the gradients p_n and q_n from n light sources. These gradients are then compared with the reference gradients p and q obtained from multi-source (all 49/55 images) PS to quantitatively determine the effect of the number and position of the light sources on the quality of PS recovery.

4.4 Intensity based Image Registration

We use an intensity based image registration method that aligns the PS images of a paper rotated in the x-y plane through 45 degrees in order to determine the geometrical accuracy of recovered surface normals by using the third data set (4-source PS).

Intensity based gradient descent, minimising the sum square difference, is used to align the raw image data. We experimented with using albedo or recovered gradient based registration but surprisingly the image based approach was equally effective despite the difference in the illumination directions used to capture the images. For simplicity we use an affine transformation model

$$\begin{pmatrix} x' \\ y' \\ 1 \end{pmatrix} = \begin{bmatrix} a_{11} & a_{12} & t_x \\ a_{21} & a_{22} & t_y \\ 0 & 0 & 1 \end{bmatrix} \begin{pmatrix} x \\ y \\ 1 \end{pmatrix}. \quad (10)$$

or simply $x' = Hx$. The transformation matrix, H, is used to map the points $(x\ y)$ in one space to the points $(x'\ y')$ in another. H contains the rotation, scale and skew parameters $(a_{11}\ a_{12}\ a_{21}\ a_{22})$ and translation in horizontal t_x and vertical t_y directions. Subsequently, the transformation matrix H is applied to the p and q gradients recovered for the rotated image data. These gradients must themselves be corrected for the rotation before they can be compared against the gradients/normals of the original images.

Let p, q, and N be the reference gradients and surface normals obtained from original photometric images. Also, p_r, q_r and N_r represent the gradients and surface normals of the registered PS data. Gradients are corrected for the rotation as follows.

$$\hat{p}_r = a_{11}p_r + a_{21}q_r \quad (11)$$

$$\hat{q}_r = a_{12}p_r + a_{22}q_r \quad (12)$$

Leading to the corrected surface normal.

$$\hat{N}_r = \frac{(-\hat{p}_r, -\hat{q}_r, 1)}{\sqrt{\hat{p}_r{}^2 + \hat{q}_r{}^2 + 1}} \quad (13)$$

The corrected and reference gradients and surface normals are then compared to determine whether at the micro-scale PS can be used to extract veridical surface normals.

5 RESULTS AND DISCUSSION

5.1 Accuracy of Sine Curve Fitting

For each paper type, we select random pixels to model using the approach outlined in Section 4.2. Figure 2 shows the result of the Sine curve fitting on random pixels of the two multi-source data sets. The top row (left-to-right) shows paper types, i.e., embossed (P1), specular (P2) and matte (P3). The middle and bottom rows show the Sine curves (corresponding to each paper type) fitted to individual random pixel of each of the two multi-source data sets of 55 and 49 images respectively. We observe that the Sine curve fits well the intensity profile at the micro-scale. In this experiment we found that the vast majority of individual pixels are well represented by a Lambertian model.

The residuals, i.e., the difference between the measured (original) pixel intensity values and the estimated values based on Lambert's model are also computed. For this purpose, we compute the root mean square error (RMS) of the reference (Original) image and the image reconstructed (using the simple PS method in Section 3 for all 49 or 55 samples), at different tilt angles, τ^k. The RMS error results obtained on the 55-source and 49-source data sets, are shown in Figure 3 left and right respectively. It can be observed from the results that a low RMS error relative to the 8 bit intensity range is obtained, i.e., most pixels are well represented by a Lambertian model. In general across both data sets we find that steeper slant angles, e.g., H=2cm and V=6cm, and H=5cm and V=6cm, give lower RMS.

5.2 Impact of Light Configuration

The procedure described in section 4.3 is applied on the two multi-source data sets in order to compute the root mean square (RMS) error of the gradients obtained from multi-source PS, and the gradients from $n = 4, 6, 8$ light sources at different subsets (size>100) of the tilt angles. In Figure 4, the RMS errors of the configurations that gave the lowest value in each case, with respect to 49-source PS, of p and q gradients are shown to demonstrate the impact of using more light sources on PS. As in previous experiments, the light source configuration H=2cm and V=6cm produces the least RMS error of

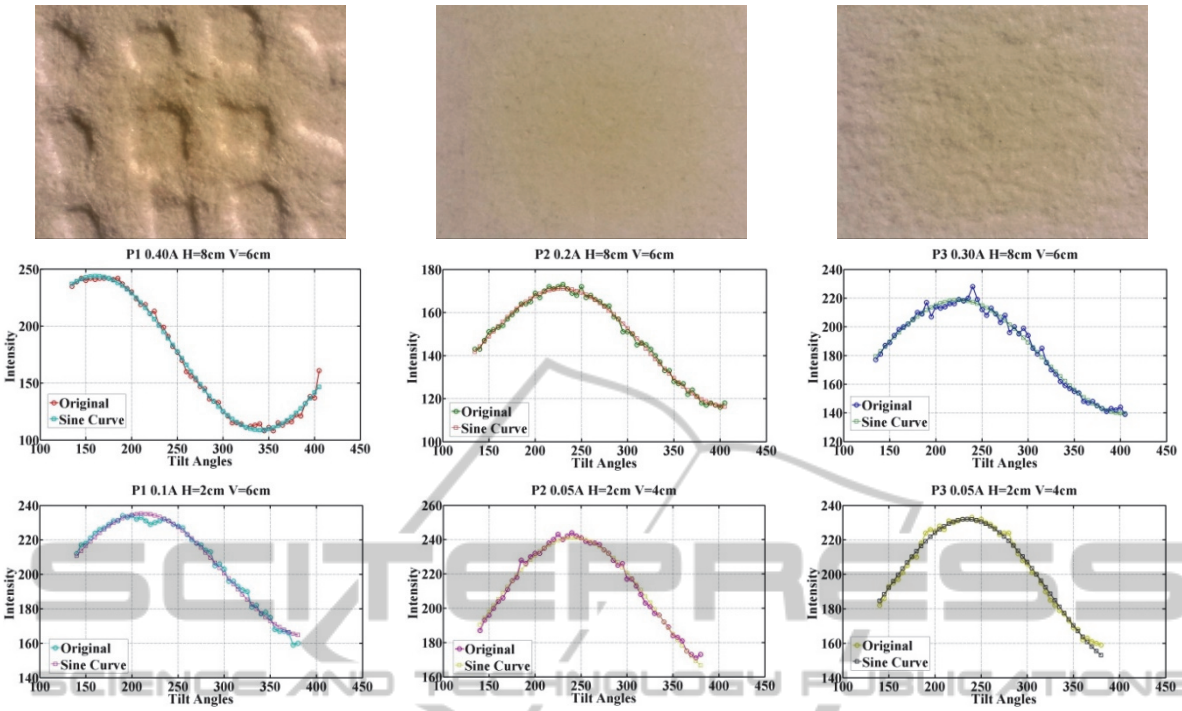

Figure 2: Sine curve fitted to the Original pixel intensity value/profile of paper illuminated from different tilt angles. Paper types, i.e., embossed (P1), specular (P2) and matte (P3), are shown in top row (left-to-right). The middle and bottom rows respectively show the corresponding Sine curves fitted to random pixels using the 55 and 49 photometric images of the two multi-source data sets. H and V are the horizontal and vertical distance of the light source from the centre of paper.

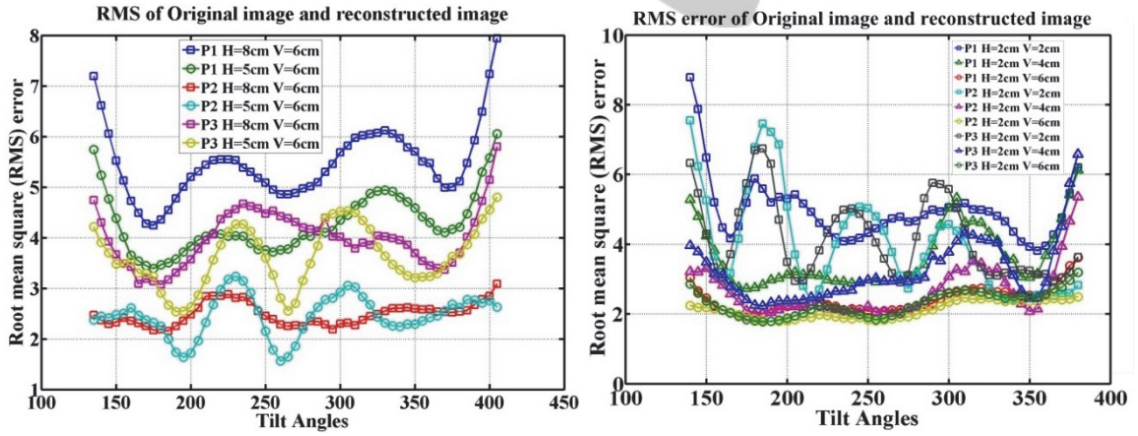

Figure 3: Root mean square (RMS) error relative to the 8 bit intensity range of the original image and reconstructed image using a Lambertian model at different light source tilt angles on 55-source and 49-source data sets in left and right respectively. H and V are the horizontal and vertical distance of the light source from the paper.

gradients for different variations of tilt angles irrespective of the number of light sources used. The number of light sources is less significant than their location with moderate improvements moving from 4 to 6 sources and a further small improvement moving on to 8 sources.

As expected configurations where the tilt angles are more evenly spread over the range of possible values tended to give lower RMS error. For 55 photometric image data set the best tilt angles in degree are [165 245 310 400], [155 210 250 295 345 395] and [150 200 220 255 290 340 375 395] for the 4, 6 and 8 light source situations with least RMS error of gradients 0.0112, 0.0101 and 0.0088 respectively. Interestingly however, the tilt angles [135 225 315 405] that are 90° degree apart could only give 0.0159.

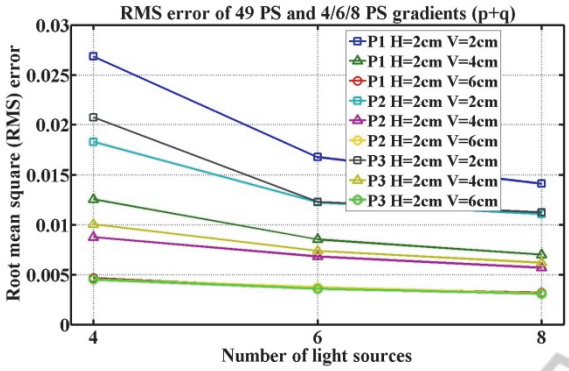

Figure 4: Root mean square (RMS) error of p and q values from best 4, 6 and 8 image PS with respect to 49 image based PS used as reference data for various illumination positions (H and V).

As expected configurations where the tilt angles are more evenly spread over the range of possible values tended to give lower RMS error. For 55 photometric image data set the best tilt angles in degree are [165 245 310 400], [155 210 250 295 345 395] and [150 200 220 255 290 340 375 395] for the 4, 6 and 8 light source situations with least RMS error of gradients 0.0112, 0.0101 and 0.0088 respectively. Interestingly however, the tilt angles [135 225 315 405] that are 90° degree apart could only give 0.0159.

5.3 Geometric Accuracy of Surface Normals

We determine whether micro-scale PS can be used to extract veridical surface normal using the procedure explained in section 4.4. The reference gradients p and q obtained from the centre region 701 x 501 pixels of the four original photometric images are compared with the gradients acquired from the registered photometric images as shown in Figure 5 (for p gradients).

For a quantitative evaluation of the reference normal N and the corrected normal $\widehat{N}_r$ we employ the angular Cosine similarity metric φ,

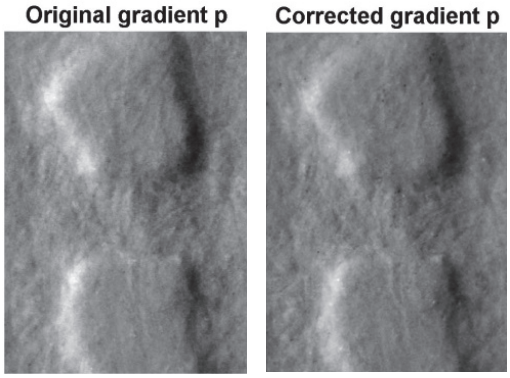

Figure 5: Reference (original) and corrected $p$gradients from the registered PS images for embossed paper.

$$\varphi = \cos^{-1}\left(\frac{N \cdot \widehat{N}_r}{\|N\|\|\widehat{N}_r\|}\right) \quad (14)$$

i.e., the angular difference between the reference and corrected normal at each pixel. In Figure 6 angular similarity of reference normals and corrected normals are shown as histograms over the centre region of the embossed (left), specular (middle) and matte (right) paper. From the small range of angles, it can be seen that PS extracts veridical surface normals in each case.

6 CONCLUSIONS

The empirical investigations in this paper show that photometric stereo (PS) based on Lambert's law represents well the paper at the micro-scale. Also, while an increase in the number of light sources resulted in a small improvement in the recovered surface gradients, the position of the light sources proved far more significant. Furthermore, PS has been shown to provide robust veridical surface normals from micro-scale paper images. These insights on the use of PS for micro-scale 3D measurement of paper will allow us in future to employ it for surface inspection, quality assurance, biometrics, shape recovery and recognition.

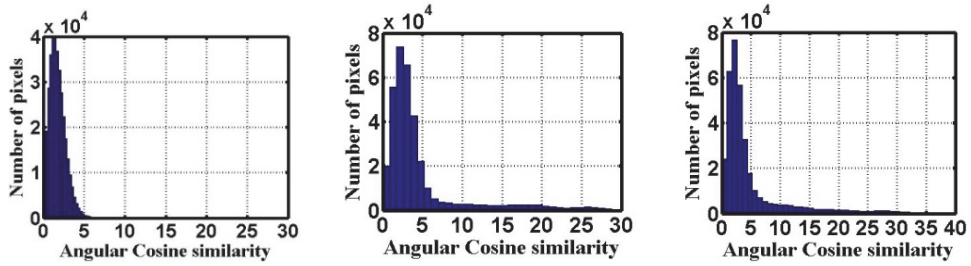

Figure 6: Angular Cosine similarity of reference normal and corrected normal on embossed, specular and matte paper left to right respectively.

REFERENCES

Angelopoulou, M.E., Petrou, M., 2013. Evaluating the effect of diffuse light on photometric stereo reconstruction. *Mach. Vis. Appl.* 25, 199–210.

Argyriou, Vasileios and Petrou, M., 2008. Photometric stereo: an overview. *Adv. Imaging Electron Phys.* 156, 1–54.

Barsky, S., Petrou, M., Sciences, P., 2003. The 4-source photometric stereo technique for 3-dimensional surfaces in the presence of highlights and shadows. *IEEE Trans. Pattern Anal. Mach. Intell.* 25, 1239 – 1252.

Bringier, B., Bony, A., Khoudeir, M., 2012. Specularity and shadow detection for the multisource photometric reconstruction of a textured surface. *J. Opt. Soc. Am. A. Opt. Image Sci. Vis.* 29, 11–21.

Chinga-carrasco, G., 2012. Complementary microscopy techniques for surface characterisation of uncoated and mineral pigment coated paper. In: *Current Microscopy Contributions to Advances in Science and Technology.* pp. 1448–1455.

Clarkson, W., Weyrich, T., Finkelstein, A., Heninger, N., Halderman, J.A., Felten, E.W., 2009. Fingerprinting Blank Paper Using Commodity Scanners. 30th *IEEE Symp. Secur. Priv.* 301–314.

Coleman, J., Jain, R.J., 1982. Obtaining 3-Dimensional Shape of Textured and Specular Surfaces Using Four-Source Photometry '. *Comput. Graph. IMAGE Process.* 18, 309–328.

Cook, R.L., Torrance, K.E., 1982. A Reflectance Model for Computer Graphics. *ACM Transanctions Graph.* 1, 7–24.

Drbohlav, O., Chantler, M., 2005. On Optimal Light Configurations in Photometric Stereo. *IEEE Int. Conf. Comput. Vis.* 2, 1707–1712.

Frankot, R.T., Chellappa, R., 1988. A method for enforcing integrability in shape from shading algorithms. *IEEE Trans. Pattern Anal. Mach. Intell.* 10, 439–451.

Gorpas, D., Kampouris, C., Malassiotis, S., 2013. Miniature photometric stereo system for textile surface structure reconstruction. *Videometrics, Range Imaging, Appl. XII; Autom. Vis. Insp.* 8791, 879117–12.

Higo, T., Matsushita, Y., Ikeuchi, K., 2010. Consensus photometric stereo. *IEEE Conf. Comput. Vis. Pattern Recognit.* 1157–1164.

Ikehata, S., Member, S., Wipf, D., 2014. Photometric Stereo Using Sparse Bayesian Regression for General Diffuse Surfaces. *IEEE Trans. Pattern Anal. Mach. Intell.* 36, 1816–1831.

Johnson, M.K., Cole, F., Raj, A., Adelson, E.H., 2011. Microgeometry capture using an elastomeric sensor. *ACM Transanctions Graph.* 30, 46:1–46:8.

Kuparinen, T., Kyrki, V., Mielikainen, J., Toivanen, P., 2007. Paper Surface Topography Using Three-light Photometric Stereo. *Conf. Mach. Vis. Appl.* 1–4.

Li, Z., Li, Y.F., 2011. Microscopic Photometric Stereo: A Dense Microstructure 3D Measurement Method. *IEEE Int. Conf. Robot. Autom.* 6009–6014.

Matsushita, Y., Ikeuchi, K., 2012. A biquadratic reflectance model for radiometric image analysis. *IEEE Conf. Comput. Vis. Pattern Recognit.* 230–237.

McGunnigle, G., Dong, J., Wang, X., 2012. Photometric stereo applied to diffuse surfaces that violate Lambert's law. *J. Opt. Soc. Am. A. Opt. Image Sci. Vis.* 29, 627–36.

Pino, A., Pladellorens, J., 2009. Measure of roughness of paper using speckle. *Proceeding SPIE* 7432, 74320E–74320E–9.

Saito, H., Omata, K., Ozawa, S., 1999. Recovery of Shape and Surface Re ectance of Specular Object from Rotation of Light Source. *Second Int. Conf. 3-D Digit. Imaging Model.* 526–535.

Sun, J., Smith, M., Smith, L., Midha, S., Bamber, J., 2007. Object surface recovery using a multi-light photometric stereo technique for non-Lambertian surfaces subject to shadows and specularities. *Image Vis. Comput.* 25, 1050–1057.

Torrance, K.E., Sparrow, E.M., 1967. Theory for Off-Specular Reflection from Roughened Surfaces. *J. Opt. Soc. Am.* 57, 1105–1114.

Woodham, R.J., 1980. Photometric method for determining surface orientation from multiple images. *Opt. Eng.* 19, 139–144.

Wu, T., Tang, C., 2010. Photometric Stereo via Expectation Maximization. *IEEE Trans. Pattern Anal. Mach. Intell.* 32, 546–560.

Yang, Q., Ahuja, N., 2012. Surface reflectance and normal estimation from photometric stereo. *Comput. Vis. Image Underst.* 116, 793–802.